Observation of seasonal variation of atmospheric multiple-muon events in the MINOS Near and Far Detectors

Article (Published Version)

Observation of seasonal variation of atmospheric multiple-muon events in the MINOS Near and Far Detectors

P. Adamson,[7] I. Anghel,[14,1] A. Aurisano,[6] G. Barr,[20] M. Bishai,[2] A. Blake,[4] G. J. Bock,[7] D. Bogert,[7] S. V. Cao,[28] C. M. Castromonte,[8] S. Childress,[7] J. A. B. Coelho,[29] L. Corwin,[13,*] D. Cronin-Hennessy,[17] J. K. de Jong,[20] A. V. Devan,[31] N. E. Devenish,[26] M. V. Diwan,[2] C. O. Escobar,[5] J. J. Evans,[16] E. Falk,[26] G. J. Feldman,[9] M. V. Frohne,[10] H. R. Gallagher,[29] R. A. Gomes,[8] M. C. Goodman,[1] P. Gouffon,[23] N. Graf,[12] R. Gran,[18] K. Grzelak,[30] A. Habig,[18] S. R. Hahn,[7] J. Hartnell,[26] R. Hatcher,[7] A. Holin,[15] J. Huang,[28] J. Hylen,[7] G. M. Irwin,[25] Z. Isvan,[2,21] C. James,[7] D. Jensen,[7] T. Kafka,[29] S. M. S. Kasahara,[17] G. Koizumi,[7] M. Kordosky,[31] A. Kreymer,[7] K. Lang,[28] J. Ling,[2] P. J. Litchfield,[17,22] P. Lucas,[7] W. A. Mann,[29] M. L. Marshak,[17] N. Mayer,[29,13] C. McGivern,[21] M. M. Medeiros,[8] R. Mehdiyev,[28] J. R. Meier,[17] M. D. Messier,[13] W. H. Miller,[17] S. R. Mishra,[24] S. Moed Sher,[7] C. D. Moore,[7] L. Mualem,[3] J. Musser,[13] D. Naples,[21] J. K. Nelson,[31] H. B. Newman,[3] R. J. Nichol,[15] J. A. Nowak,[17] J. O'Connor,[15] M. Orchanian,[3] S. Osprey,[20] R. B. Pahlka,[7] J. Paley,[1] R. B. Patterson,[3] G. Pawloski,[17,25] A. Perch,[15] S. Phan-Budd,[1] R. K. Plunkett,[7] N. Poonthottathil,[7] X. Qiu,[25] A. Radovic,[31] B. Rebel,[7] C. Rosenfeld,[24] H. A. Rubin,[12] M. C. Sanchez,[14,1] J. Schneps,[29] A. Schreckenberger,[28,17] P. Schreiner,[1] R. Sharma,[7] A. Sousa,[6,9] N. Tagg,[19] R. L. Talaga,[1] J. Thomas,[15] M. A. Thomson,[4] X. Tian,[24] A. Timmons,[16] S. C. Tognini,[8] R. Toner,[9,4] D. Torretta,[7] J. Urheim,[13] P. Vahle,[31] B. Viren,[2] A. Weber,[20,22] R. C. Webb,[27] C. White,[12] L. Whitehead,[11,2] L. H. Whitehead,[15] S. G. Wojcicki,[25] and R. Zwaska[7]

(MINOS Collaboration)

[1]*Argonne National Laboratory, Argonne, Illinois 60439, USA*
[2]*Brookhaven National Laboratory, Upton, New York 11973, USA*
[3]*Lauritsen Laboratory, California Institute of Technology, Pasadena, California 91125, USA*
[4]*Cavendish Laboratory, University of Cambridge, Madingley Road, Cambridge CB3 0HE, United Kingdom*
[5]*Universidade Estadual de Campinas, IFGW-UNICAMP, CP 6165, 13083-970 Campinas, SP, Brazil*
[6]*Department of Physics, University of Cincinnati, Cincinnati, Ohio 45221, USA*
[7]*Fermi National Accelerator Laboratory, Batavia, Illinois 60510, USA*
[8]*Instituto de Física, Universidade Federal de Goiás, CP 131, 74001-970 Goiânia, GO, Brazil*
[9]*Department of Physics, Harvard University, Cambridge, Massachusetts 02138, USA*
[10]*Holy Cross College, Notre Dame, Indiana 46556, USA*
[11]*Department of Physics, University of Houston, Houston, Texas 77204, USA*
[12]*Department of Physics, Illinois Institute of Technology, Chicago, Illinois 60616, USA*
[13]*Indiana University, Bloomington, Indiana 47405, USA*
[14]*Department of Physics and Astronomy, Iowa State University, Ames, Iowa 50011 USA*
[15]*Department of Physics and Astronomy, University College London, Gower Street, London WC1E 6BT, United Kingdom*
[16]*School of Physics and Astronomy, University of Manchester, Oxford Road, Manchester M13 9PL, United Kingdom*
[17]*University of Minnesota, Minneapolis, Minnesota 55455, USA*
[18]*Department of Physics, University of Minnesota Duluth, Duluth, Minnesota 55812, USA*
[19]*Otterbein College, Westerville, Ohio 43081, USA*
[20]*Subdepartment of Particle Physics, University of Oxford, Oxford OX1 3RH, United Kingdom*
[21]*Department of Physics and Astronomy, University of Pittsburgh, Pittsburgh, Pennsylvania 15260, USA*
[22]*Rutherford Appleton Laboratory, Science and TechnologiesFacilities Council, Didcot OX11 0QX, United Kingdom*
[23]*Instituto de Física, Universidade de São Paulo, CP 66318, 05315-970 São Paulo, SP, Brazil*
[24]*Department of Physics and Astronomy, University of South Carolina, Columbia, South Carolina 29208, USA*
[25]*Department of Physics, Stanford University, Stanford, California 94305, USA*
[26]*Department of Physics and Astronomy, University of Sussex, Falmer, Brighton BN1 9QH, United Kingdom*
[27]*Physics Department, Texas A&M University, College Station, Texas 77843, USA*
[28]*Department of Physics, University of Texas at Austin, 1 University Station C1600, Austin, Texas 78712, USA*

1550-7998/2015/91(11)/112006(9)

[29]Physics Department, Tufts University, Medford, Massachusetts 02155, USA
[30]Department of Physics, University of Warsaw, Pasteura 5, PL-02-093 Warsaw, Poland
[31]Department of Physics, College of William and Mary, Williamsburg, Virginia 23187, USA
(Received 31 March 2015; published 9 June 2015)

We report the first observation of seasonal modulations in the rates of cosmic ray multiple-muon events at two underground sites, the MINOS Near Detector with an overburden of 225 mwe, and the MINOS Far Detector site at 2100 mwe. At the deeper site, multiple-muon events with muons separated by more than 8 m exhibit a seasonal rate that peaks during the summer, similar to that of single-muon events. In contrast and unexpectedly, the rate of multiple-muon events with muons separated by less than 5–8 m, and the rate of multiple-muon events in the smaller, shallower Near Detector, exhibit a seasonal rate modulation that peaks in the winter.

DOI: 10.1103/PhysRevD.91.112006 PACS numbers: 95.55.Vj, 13.85.Tp, 98.70.Sa, 98.70.Vc

I. INTRODUCTION

Muons observed in underground particle detectors originate from the interactions of cosmic rays with nuclei in the upper atmosphere. These interactions produce pions (π) and kaons (K) which can either interact, generating hadronic cascades, or decay, producing muons. The probability that these mesons will decay rather than interact is dependent on their energy and the density of the atmosphere near their point of production. The temperature of the upper atmosphere varies slowly over the year, causing a seasonal effect on underground muon rates. Increases in the temperature of the atmosphere decrease the local density and thus reduce the probability that a secondary meson will interact. Consequently, the muon flux should increase in the summer. A number of experiments have observed this variation in the single-muon rate [1–11], including MINOS in both Far Detector (FD) data [12,13] and Near Detector (ND) data [14].

Seasonal variations for single muons have been studied with a correlation coefficient α_T defined by

$$\frac{\Delta R_\mu}{\langle R_\mu \rangle} = \alpha_T \frac{\Delta T_{\text{eff}}}{\langle T_{\text{eff}} \rangle} \tag{1}$$

where $\langle R_\mu \rangle$ is the mean muon rate, and is equivalent to the rate for an effective atmospheric temperature equal to $\langle T_{\text{eff}} \rangle$. The magnitude of the temperature coefficient α_T is dependent on the muon energy at production and hence the depth of the detector. The effective temperature T_{eff} is a weighted average over the region of the atmosphere where the muons originate.

By the same reasoning as above a variation should also be present in the rate of multiple-muon events. No such studies of multiple-muon seasonal rates are reported in the literature. The formulas used to calculate T_{eff} for single muons assume a single leading hadron from the first interaction is the parent, an assumption that is not applicable for multiple-muon events.

The probability that a cosmic ray shower will give a multiple-muon event observed in the MINOS Near or Far Detectors is enhanced whenever any of the following conditions are true: (1) The primary interaction occurs high in the atmosphere where the density is lower and a larger fraction of produced hadrons decay, (2) the energy of the primary is large so a higher multiplicity of hadrons is produced, (3) the cosmic ray primary is a heavy nucleus which breaks up and makes more hadrons, and (4) a leading hadron decays to dimuons. Assuming the relative probability of interaction and decay for each meson in a shower is independent, for multiple muons that come from the same energy and altitude as a single-muon event, one might expect an increase in rate during the summer that is roughly proportional to the muon multiplicity, m_μ, such that $\alpha_{T,N} = m_\mu \times \alpha_{T,1}$. The result presented here differs greatly from this. This paper presents the first measurement of the multiple-muon modulation parameters.

Note that most extensive air showers have many muons in them, but that the highest energy muons which can reach an underground detector are produced in the first few interactions. Observed single-muon events are most likely multiple muons in which any other muons range out before reaching the detector or missed the detector laterally. A single muon observed in a detector underground is most likely the highest energy muon from the shower due to the steeply falling cosmic ray energy spectrum.

The MINOS detectors and the event selection are described in Sec. II. In Sec. III the measurement and comparison of the modulation parameters for the MINOS ND and FD multiple-muon and single-muon event rates are presented. In Sec. IV and Sec. V some possible explanations of the seasonal behavior of the multiple-muon rates are considered.

II. THE MINOS DETECTORS AND MUON DATA

The MINOS detectors are planar magnetized steel/scintillator tracking calorimeters [15]. The vertically oriented detector planes are composed of 2.54 cm thick steel

[*]Present address: South Dakota School of Mines and Technology, Rapid City, South Dakota 57701, USA.

and 1 cm thick plastic scintillator. A scintillator layer is composed of 4.1 cm wide strips. The MINOS ND has a total mass of 0.98 kton, and lies 104 m (225 mwe) underground at Fermilab at 42° north latitude. The detector is made from 3.8×4.8 m hexagonal planes and is 17 m long. It consists of two sections, a calorimeter encompassing the upstream 121 planes and a spectrometer containing the downstream 161 planes. In both sections, one out of every five planes is covered with 96 scintillator strips attached to the steel planes. In the calorimeter section, the other four out of five planes are covered with 64 scintillator strips, while in the spectrometer section they have no scintillator. Only muons which enter the calorimeter are included in this analysis. The larger FD is 705 m below the surface (2100 mwe), has a total mass of 5.4 kton, and is located in the Soudan Underground Laboratory, at 48° north latitude. It is composed of 484 steel-scintillator 8.0 m octagonal planes and is 31 m long. The detectors are oriented to face the NuMI beam, but through-going cosmic muons are well reconstructed over wide geometric angular regions.

Six years of MINOS ND data collected between June 1, 2006 and April 30, 2012 and 9 years of MINOS FD data collected between August 1, 2003 and April 30, 2012 are analyzed for this paper. The cosmic muon trigger criteria are similar at both detectors requiring that a signal is registered in either 4 strips in 5 sequential planes or that strips from any 20 planes register a total signal above threshold within a given time window. The raw cosmic trigger rate at the ND and FD are approximately 27 and 0.5 Hz respectively.

The single-muon event selection requires there to be a single reconstructed track in an event. The multiple-muon event selection requires there to be more than one reconstructed track in an event. However, since the single-muon event rate is much larger than the multiple-muon event rate, the multiple-muon sample contains a background of single-muon events that have been misreconstructed to contain two tracks. This background is greatly reduced by requiring that, for multi-track events, the track separation, ΔS, defined as the minimum distance of closest approach between any two tracks, be greater than 0.6 m. Observed excesses due to this background at small ΔS in both the ND and FD were removed by this selection, reducing the background from 1.3% to less than 200 events out of 11 million in the FD. Figure 1 shows the time between sequential multiple-muon events. The multiple-muon event rates at the ND and FD are 19.6 and 14.1 mHz respectively. In total the MINOS ND and FD have collected 2.45×10^6 and 3.36×10^6 good multiple-muon events respectively.

The rate of multiple muons in the MINOS detectors is dominated by $m_\mu = 2$ and $m_\mu = 3$, where m_μ is the muon multiplicity. For the FD, the reconstruction works well for these small multiplicities, identifying all tracks in 84% (67%) of events for $m_\mu = 2(3)$. From a multiple-muon Monte Carlo [16], the efficiency for identifying an event as

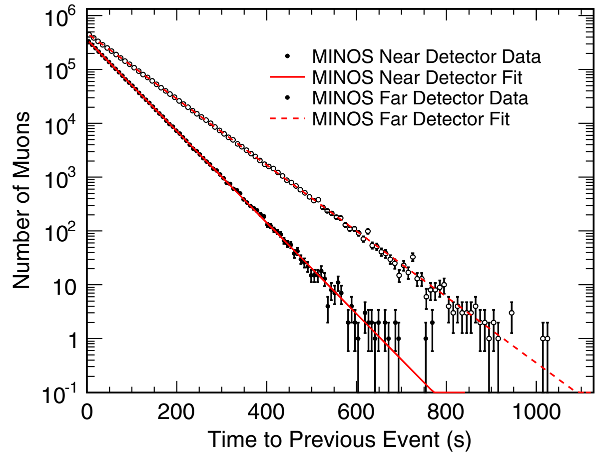

FIG. 1 (color online). Time between neighboring atmospheric multiple-muon events in the MINOS detectors. The data are well described by an exponential over 6 orders of magnitude in instantaneous rate.

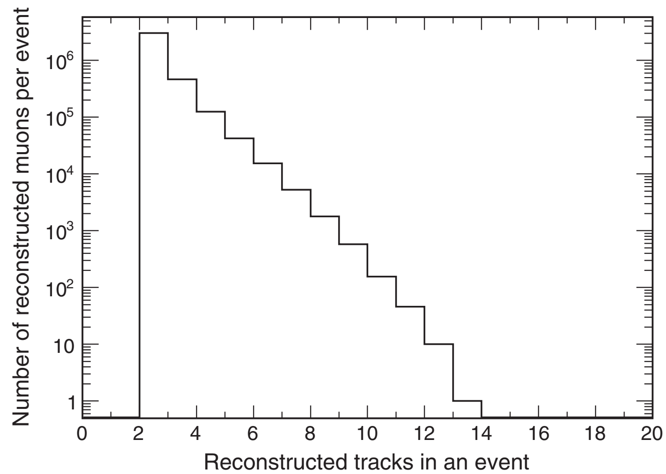

FIG. 2. The reconstructed muon multiplicity data, for events containing more than one reconstructed track, in the Far Detector.

a multiple muon is 84% (94%) for $m_\mu = 2(3)$, rising to above 97% for $m_\mu > 3$. However, the reconstructed multiplicity is frequently too low for high-multiplicity events. No event with $m_\mu > 13$ is recorded in either of the MINOS detectors. Similar measurements with the finer-grained Soudan 2 detector at the same depth as the MINOS FD recorded multiplicities up to 20 [17]. In the coarser-grained MINOS detectors, the individual tracks closest in distance from such high-multiplicity events will be resolved as a single track or not pass the track quality criteria used in the MINOS reconstruction algorithms. Figure 2 shows the reconstructed multiplicity distribution in the MINOS FD.

III. MODULATION ANALYSIS

To compare the variation in the event rates for multiple-muon and single-muon events, the rates are fit to a

TABLE I. The parameters obtained when Eq. (2) is fit to the single-muon and multiple-muon data in each detector. The table also shows the results of fits to subsets of the multiple-muon data, based on the minimum separation between tracks. The best-fit phase and period do not change significantly if the loss rate is assumed to be zero.

Data set	Region	Amplitude (%)	Loss rate (f) (%/year)	Period (T) (days)	Phase (t_0) (days)
		MINOS FD			
$\Delta S > 0.6$ m	ABC	0.39 ± 0.08	-0.04 ± 0.02	356.4 ± 4.1	105.2 ± 16.1
0.6 m $< \Delta S < 4.5$ m	A	1.0 ± 0.1	-0.14 ± 0.04	362.2 ± 3.3	27.6 ± 8.9
4.5 m $< \Delta S < 8.0$ m	B	0.47 ± 0.14	0.02 ± 0.04	354.6 ± 9.1	78.9 ± 17.3
$\Delta S > 8.0$ m	C	2.0 ± 0.1	0.01 ± 0.04	363.7 ± 1.8	184.8 ± 6.5
Single muons		1.27 ± 0.01	0.013 ± 0.001	364.4 ± 0.3	183.0 ± 0.9
		MINOS ND			
$\Delta S > 0.6$ m	ABC	2.51 ± 0.09	0.35 ± 0.03	367.4 ± 1.3	23.7 ± 2.3
0.6 m $< \Delta S < 1.8$ m	A	2.35 ± 0.17	0.25 ± 0.05	369.0 ± 2.5	26.2 ± 4.2
1.8 m $< \Delta S < 3.0$ m	B	2.53 ± 0.17	0.41 ± 0.05	369.3 ± 2.3	25.1 ± 4.0
$\Delta S > 3.0$ m	C	2.64 ± 0.17	0.39 ± 0.05	365.8 ± 2.1	22.1 ± 3.8
Single muons		0.268 ± 0.004	0.0116 ± 0.001	365.7 ± 0.4	198.6 ± 0.9

sinusoidally varying function of time. There is no *a priori* reason to believe that the rates vary sinusoidally through the year, but this fit gives a qualitatively useful amplitude and phase. The following function, which contains four free parameters, is used for the fit:

$$R(t) = R_0\left(1 - \frac{ft}{365.25}\right)\left(1 + A\cos\left[\frac{2\pi}{T}(t - t_0)\right]\right) \quad (2)$$

where t is the number of days since Jan. 1, 2010 and t_0 is the phase, R_0 is the mean rate on Jan. 1, 2010, A is the modulation amplitude and T is the period (approximately 1 year). The parameter f is the loss rate that accounts for an observed linear decrease in the event rate in both the FD and ND over the lifetime of the experiment. Possible explanations for this small but apparently steady decrease are discussed in Ref. [14]. Although no conclusive explanation is found, the effect is too small to affect the energy scale in neutrino data analyses, and does not affect the conclusions of the muon data analysis described in this paper. The best-fit parameters are given in Table I.

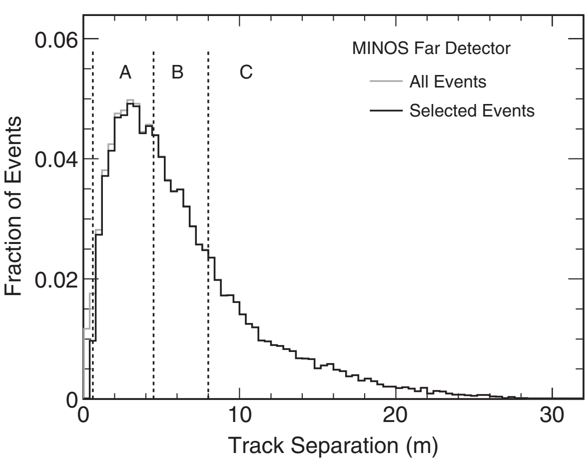

FIG. 3. The minimum track separation ΔS between any two tracks in multiple-muon events recorded in the FD. The gray (black) histogram is the distribution before (after) the selection to remove misreconstructed single-muon events. Regions of track separation ΔS are defined as A: 0.6–4.5 m, B: 4.5–8.0 m and C: > 8 m.

A. Modulations in the Far Detector

The fit for seasonal variations in the FD multiple-muon sample shows a much smaller amplitude than for single muons, and a poorly defined phase. Since the MINOS FD is larger than the ND and is fully instrumented, the modulation is studied as a function of track separation. Figure 3

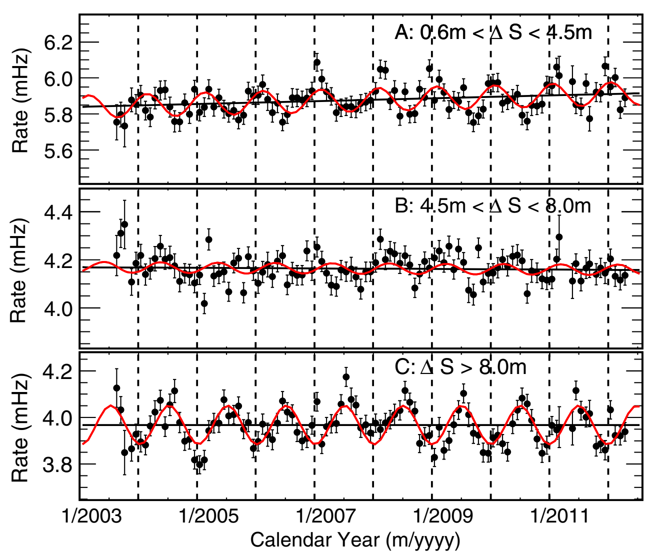

FIG. 4 (color online). The multiple-muon rate in the FD as a function of time for different track separations. Each data point corresponds to one calendar month of data. The solid red lines are the best fit to Eq. (2). The top graph is for the smallest track separation, the middle graph for midrange and the bottom graph for the largest. The vertical lines are year boundaries and the solid horizontal line represents the fit without the cosine term.

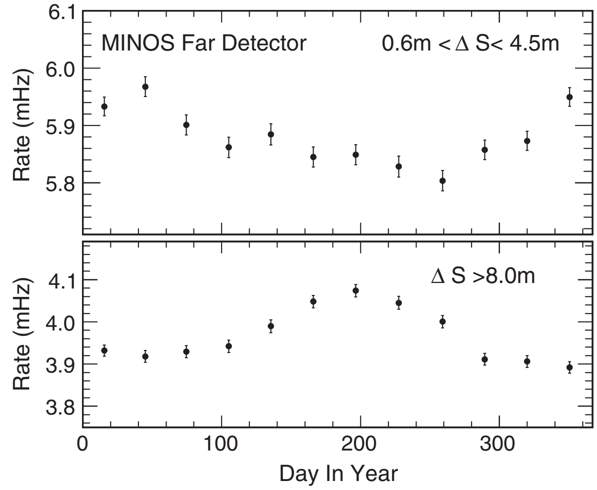

FIG. 5. The multiple-muon rate in the FD for events with ΔS range A from 0.6 to 4.5 m (top graph) and for events with ΔS range C larger than 8 m (bottom) binned according to calendar month. The top figure shows a winter maximum. The bottom figure shows a summer maximum.

shows the track separation ΔS. The multiple-muon data are grouped into three bins of roughly equal statistics with track separations from 0.6–4.5 m (FD region A), 4.5–8.0 m (FD region B) and greater than 8 m (FD region C). Region A most closely resembles the distribution in the ND.

Figure 4 presents the multiple-muon rate in the MINOS FD as a function of time for differing track separations. The FD multiple-muon data set with the largest track separation, > 8 m, modulates with a summer maximum ($t_0 = 184.8 \pm 6.5$ days); this phase is consistent with that observed in the FD single-muon sample, and the amplitude is larger. On the other hand, the FD multiple-muon data set with the smallest track separations modulates with

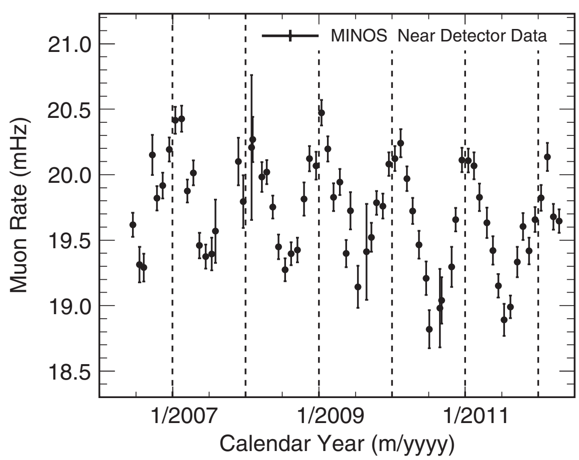

FIG. 6. The multiple-muon rate in the ND as a function of time. Each data point corresponds to one calendar month. A clear modulation in the data is observed with the maximum occurring towards the start of the year. The vertical lines are year boundaries.

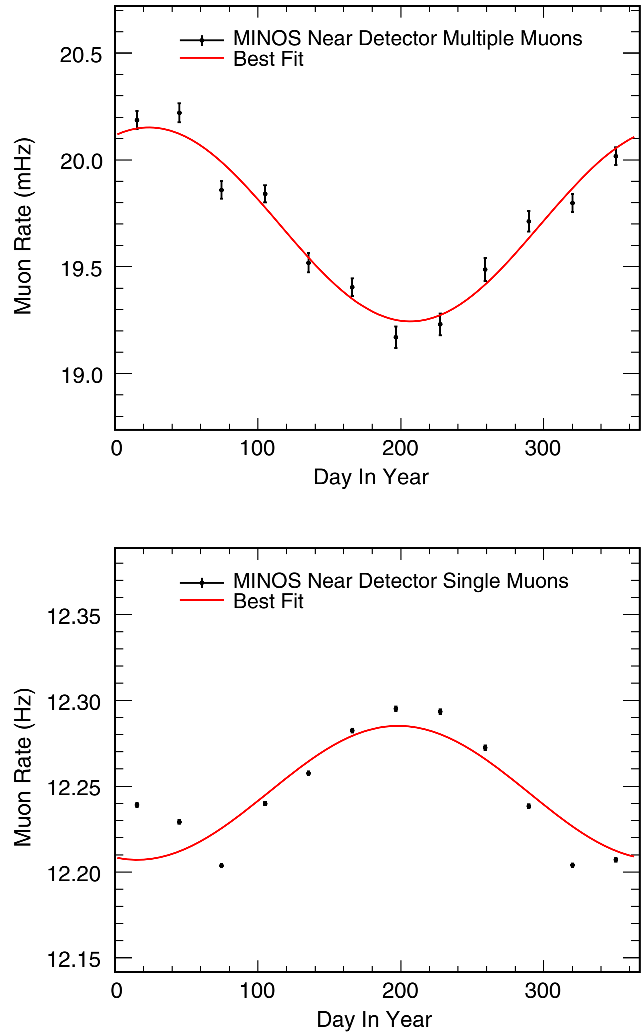

FIG. 7 (color online). The top figure is the multiple-muon rate in the ND, binned according to calendar month, which each point showing the average rate for all years of data taking. The figure also shows a cosine fit to the data. The single-muon rate is shown in the bottom figure, showing a clearly different seasonal modulation.

a winter maximum ($t_0 = 27.6 \pm 8.9$ days); this phase differs by a half year from the variation seen with single muons. The FD midrange track-separation multiple-muon data set has a small amplitude and is consistent with an admixture of the other two phases.

In Fig. 5, the data for regions A and C have been binned by calendar month, with each point showing the average rate over all years of data taking.

B. Modulations in the Near Detector

The ND multiple-muon data, shown in Fig. 6, and the single-muon data (shown in Ref. [14]) were fit to Eq. (2) using one month time interval bins. The multiple-muon event rate data show a clear modulation signature. However, unlike the single-muon rate which reaches its

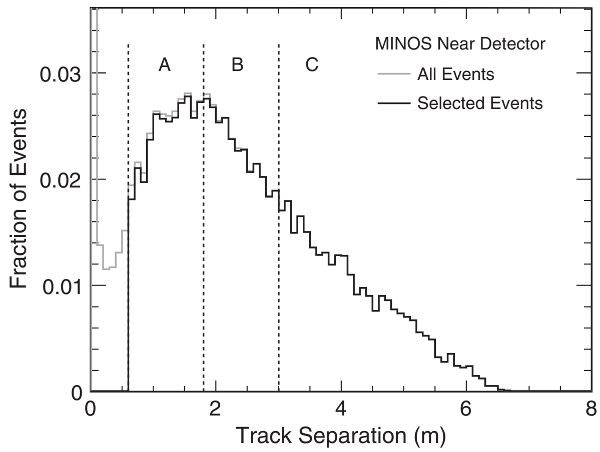

FIG. 8. The minimum track separation ΔS between any two tracks in multiple-muon events recorded in the ND. The gray (black) histogram is the distribution before (after) the selection to remove misreconstructed single-muon events. Regions of track separation ΔS are defined as A: 0.6–1.8 m, B: 1.8–3.0 m and C: > 3 m.

maximum in the summer [14], the multiple-muon rate reaches its maximum in the winter. This also matches the modulation for the region-A multiple muons in the FD. Both the single-muon and multiple-muon data sets have periods consistent with one year but their phases, 198.6 ± 0.9 days and 23.7 ± 2.3 days respectively, differ by about six months. The rates of multiple muons and single muons, binned by calendar month and averaged over all years of data taking, are shown in Fig. 7.

Figure 8 shows the track separation in ND multiple-muon events. To qualitatively match the procedure in the FD, the data have been grouped into three bins of roughly equal statistics with track separations of 0.6–1.8 m (ND region A), 1.8–3.0 m (ND region B) and greater than 3 m (ND region C). As before, the data are fit to Eq. (2) and the best-fit parameters are given in Table I. There is no apparent difference in the fit parameters for the three ND regions, which all peak in the winter. There is consistency between ND regions ABC and FD region A in both ΔS and a winter maximum.

IV. DISCUSSION OF RESULTS AND POSSIBLE EXPLANATIONS

We have previously observed seasonal variations in single-muon rates in the MINOS ND and FD that correlate at expected levels with the temperature changes and the season. Those muon rates rose in the summer as did the calculated values of T_{eff}, and the measured correlations were $\alpha_T^{\mathrm{ND}} = 0.428 \pm 0.059$ [14] and $\alpha_T^{\mathrm{FD}} = 0.873 \pm 0.014$ [13]. The measurement of a multiple-muon rate in the ND that peaks in the winter is unexpected, as is the winter maximum in the FD in region A of separation. In order to try to understand this result, four plausible explanations

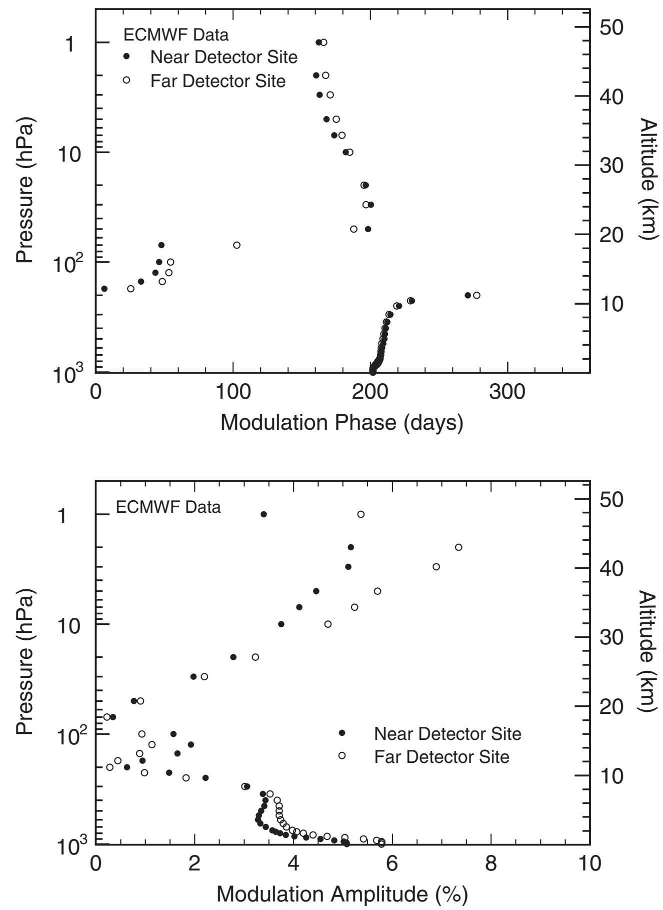

FIG. 9. The (top) modulation phase relative to 1 Jan. and (bottom) amplitude in the ECMWF temperature data based on a cosine fit are shown as a function of altitude and detector site. These distributions were used to study both the geometry effect (B) and the temperature effect (C). The five points on the left in the top figure show a portion of the atmosphere with a winter maximum temperature, albeit with a small amplitude as indicated in the lower figure.

which might account for these results are considered. They involve (A) a source of dimuons from prompt hadron decays (such as η and ρ) that may have the opposite seasonal variation, since in the winter the secondary pions are more likely to interact than decay and produce more of such hadrons, (B) a geometric effect in which different altitude distributions affect the track separation underground, (C) a different altitude distribution for multimuon events that may come from regions of the atmosphere with different seasonal temperature profiles, and (D) leading secondary hadrons being more likely to decay than interact in the summer, and thus less likely to make multiple hadrons which make multiple muons. We discuss each of these possibilities in the current section.

A. Hadronic dimuon decays

One idea is that the winter maximum may be due to hadronic decays into dimuons. In the winter, while pions are less likely to decay in the atmosphere, the decay probability of other hadrons which have dimuon decays, such as η and ρ mesons, changes negligibly. The 2% more pions [13] which interact will increase the number of these other hadrons. This increase, which is at most 2%, must then be folded in with the small dimuon branching ratios, such as 4.6×10^{-5} for $\rho \to \mu^+\mu^-$ and 3.1×10^{-4} for $\eta \to \mu^+\mu^-\gamma$ [25]. Observed dimuon rates are 1% of the single-muon rates in the FD, and 0.16% in the ND, so even if ρ and η production were comparable to π, this contribution is at most 6×10^{-6}, too small to account for the observed effect.

B. A geometry effect

A possibility is that the muons generated higher in the atmosphere in the summer spread out farther so that there are fewer of them in region A. This would be solely a geometric effect, in that it would not affect the number of multimuons in each season but only the track-separation distribution. This is further complicated by multiple scattering, but an effect due to the opening angle at production can be estimated. For a fixed-size detector, a difference in the track-separation distribution would affect the measured rate. The altitude of the first interaction in an isothermal atmosphere is related to the absolute temperature. A $\pm 2\%$ seasonal change in the effective temperature would cause a $\pm 2\%$ change in the altitude, and hence less than a 4% change in the average muon track separation underground. This would move events to the right in Fig. 3. Due to the shape of the distribution, more events would move from region A to region B than from region B to region C, which is in contradiction to our fits. Also, one would expect a similar effect in the ND, but as shown in Table I, the track-separation dependence is not seen.

C. A temperature effect

To determine whether there may be an altitude-dependent seasonal variation that differs for single and multiple muons, meteorological data is used to determine the atmospheric temperature profile. Figure 9 gives the phase and amplitude of the modulation of the atmospheric temperature, based on a cosine fit to data taken from the European Center for Medium-Range Weather Forecasts (ECMWF) model [18], as a function of atmospheric pressure. Indeed, there is a small region of the atmosphere, between 70 and 175 hPa, where the temperature reaches a maximum in the winter. Note, however, the small amplitude of the annual temperature variation at those altitudes.

In order to study the possible altitude dependence of multiple muons we simulated cosmic ray air showers which could make multiple muons in the MINOS FD. The Monte Carlo sample was produced by CORSIKA [19,20] using version 7.4. We have run CORSIKA with three different hadronic models, QGSJET-01C, QGSJET II-04 [21] and EPOS [22] which gave consistent results. We note that CORSIKA uses an isothermal atmosphere and cannot be used per se to study seasonal variations [23]. The goal here is to roughly calculate the altitude dependence for the three regions of track separation. CORSIKA outputs muon energies and positions at the earth's surface. To reach the MINOS FD, energy loss through the rock was calculated using [24]

$$E_{\text{loss}}(X) = \frac{a}{b_T}(e^{b_T X} - 1), \qquad (3)$$

where X is the rock overburden, a is a parameter for the ionization energy loss and $b_T = b_{\text{brem}} + b_{\text{pair}} + b_{\text{DIS}}$ represents the energy loss due to bremsstrahlung, electron-positron pair production and photo-nuclear interactions.

Simulated events were selected for which two or more muons reached the top of the FD with a total remaining energy of at least 0.9 GeV. The distribution of track separation obtained with this simulation was similar to, but not identical to, the distribution seen in data (Fig. 3). We then extracted from CORSIKA the altitude at which each muon was created in each track-separation region. Those three distributions are shown in Fig. 10. There is a shift in the mean altitude for each region of track separation from 17 km in region A to 21 km in region C, though all three distributions are quite broad. We then combined the altitude dependence with the temperature phase and amplitude fits shown in Fig. 9, assuming the rate and T_{eff} were completely correlated, to compare the overall variation of T_{eff} averaged over each track-separation region. The result was a variation that peaked in the summer in all three regions, with an amplitude of 1.9% in region C and 1.6% in regions A and B. This study was repeated using QGSJET-01C, QGSJET II and EPOS and all three results were similar.

If all multiple muons originated between 10 and 18 km where Fig. 9 shows a winter maximum, there would have been a multiple-muon rate with a small winter maximum. The small temperature amplitude at those altitudes together with the much wider altitude distribution show that this is

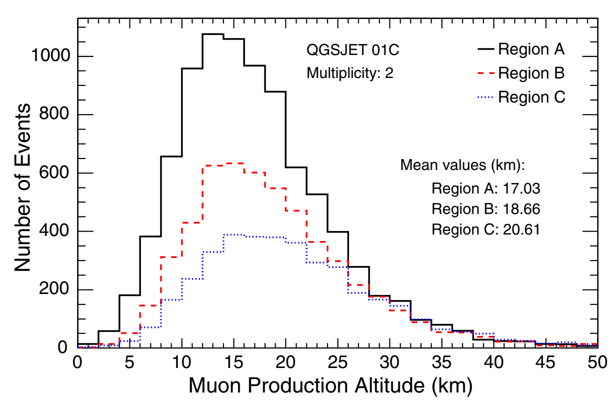

FIG. 10 (color online). To study a possible temperature effect with altitude, (Sec. IV C in the text), the altitude distribution from CORSIKA for MINOS FD multiple muons are shown for each of the three regions of track separation in Fig. 3.

not the case. It does not appear that the temperature variations noted in Fig. 9 can account for the observed reverse seasonal effect in region A.

D. Anticorrelation of primary and secondary decays

As a last hypothesis, while most single-muon events come from secondary pions and kaons produced in the primary cosmic ray interaction, multiple muons may be more likely to come from higher energy primaries where there are further hadronic interactions deeper in the shower. In that case, if the secondary hadron is more likely to decay in the summer, it is less likely to interact and make additional pions and kaons which contribute to multiple muons. This may be the best explanation for the winter maximum measured in the MINOS ND multiple-muon data set. A quantitative test of this hypothesis will require a detailed study of air-shower development that is beyond the scope of this analysis. This hypothesis accounts for the stronger effect in the MINOS ND, where the muons come from pions and kaons below their critical energies ($\epsilon_\pi = 115$ GeV and $\epsilon_K = 850$ GeV, defined as those energies for which meson decay and interaction rates in the atmosphere where muons originate are equal) [1] and for the more complex effect in the MINOS FD where the energies are above ϵ_π and comparable to ϵ_K. Mesons which are much below their critical energies mostly decay, so the temperature effect that does exist to increase the decay rate in the summer has a large effect on decreasing the interaction rate in the summer. This is the situation for muons in the ND where the threshold from the overburden is near 50 GeV. At the FD, where the threshold is almost a TeV, a change in the decay rate has a smaller impact on the interaction rate, since a large fraction of the hadrons are interacting before they decay.

As pointed out in the Introduction, single muons come predominantly from the decay of a leading hadron, and multiple muons from a more complicated process. It is clear that if a leading hadron is more likely to decay in one season, it is less likely to interact.

V. CONCLUSION

We have shown evidence of an annual modulation in the MINOS ND multiple-muon data set in which the maximum rate occurs in the winter. This phase is inconsistent with the summer maximum observed in the ND and FD single-muon data. Data collected by the MINOS FD were used to show that there is a transition from a summer maximum in multiple-muon events with a large track separation to a winter maximum in multiple-muon events with a small track separation. This transition occurs at track separations of about 5–8 m.

Four possible explanations for this observed characteristic in seasonal variations were considered. One explanation is favored: This is a hypothesis in which multiple muons come preferentially from higher energy pions and kaons which, in the summer, are less likely to interact and produce the secondary pions and kaons that give rise to the multiple muons. However, a full explanation of our observations including the dependence in the FD on track separation must come from a more detailed study of extensive air-shower properties and the properties of the atmosphere.

ACKNOWLEDGMENTS

This work was supported by the U.S. DOE, the United Kingdom STFC, the U.S. NSF, the state and University of Minnesota, and Brazil's FAPESP, CNPq and CAPES. We are grateful to the Minnesota Department of Natural Resources and the personnel of the Soudan Laboratory and Fermilab for their contributions to the experiment. Fermilab is operated by Fermi Research Alliance, LLC under Contract No. De-AC02-07CH11359 with the United States Department of Energy.

[1] P. H. Barrett, L. M. Bollinger, G. Cocconi, Y. Eisenberg, and K. Greisen, Rev. Mod. Phys. **24**, 133 (1952).
[2] G. Castagnoli and M. A. Dodero, Il Nuovo Cim. B **51**, 525 (1967).
[3] N. Sherman, Phys. Rev. **93**, 208 (1954).
[4] G. C. Castagnoli and M. Dodero (Torino Collaboration), Rev. Mod. Phys. **24**, 133 (1952).
[5] A. Fenton, R. Jacklyn, and R. Taylor, Il Nuovo Cim. **22**, 285 (1961).
[6] Y. Andreyev *et al.* (Baksan Collaboration), in *Proceedings of the 20th ICRC* (Moscow NAUKA, Moscow Soviet Union, 1987), Vol. 3, p. 270.
[7] M. Ambrosio *et al.* (MACRO Collaboration), Astropart. Phys. **7**, 109 (1997).
[8] A. Bouchta (AMANDA Collaboration), in *Proceedings of the 26th ICRC* edited by D. Kieda, M. Salamon, and B. Dingus, (Salt Lake City, 1999), Vol. 2, pp. 108–111.
[9] G. Bellini *et al.* (Borexino Collaboration), J. Cosmol. Astropart. Phys. 05 (2012) 015.
[10] M. Selvi (LVD Collaboration), in *Proceedings of the 31st ICRC* (Lodz, 2009), http://icrc2009.uni.lodz.pl/proc/html/.
[11] P. Desiati *et al.* (IceCube Collaboration), in *Proceedings of the 32nd ICRC* (Beijing, 2011), http://www.ihep.ac.cn/english/conference/icrc2011/paper/.

[12] S. Osprey *et al.* (MINOS Collaboration), Geophys. Res. Lett. **36**, L05809 (2009).
[13] P. Adamson *et al.* (MINOS Collaboration), Phys. Rev. D **81**, 012001 (2010).
[14] P. Adamson *et al.* (MINOS Collaboration), Phys. Rev. D **90**, 012010 (2014).
[15] D. G. Michael *et al.* (MINOS Collaboration), Nucl. Instrum. Methods Phys. Res., Sect. A **596**, 190 (2008).
[16] P. Adamson *et al.* (MINOS Collaboration) (to be published).
[17] S. Kasahara *et al.* (Soudan 2 Collaboration), Phys. Rev. D **55**, 5282 (1997).
[18] European Centre for Medium-Range Weather Forecasts ECMWF Operational Analysis data, [Internet] British Atmospheric Data Centre, 2006-2007, available from http://badc.nerc.ac.uk/data/ecmwf-op/.
[19] D. Heck *et al.*, Extensive Air Shower Simulation with CORSIKA: A User's Guide, available at http://www.ikp.kit.edu/corsika/.
[20] D. Heck *et al.*, Report No. FZKA 6019.
[21] S. Ostapchenko, Phys. Rev. D **83**, 014018 (2011).
[22] K. Werner, F.-M. Liu, and T. Pierog, Phys. Rev. C **74**, 044902 (2006).
[23] S. Tognini, M.S. thesis, Federal University of Goias, 2012.
[24] J. Reichenbacher and M. Goodman, in *Proceedings of the 30th ICRC* (Merida, 2008), http://www.icrc2007.unam.mx/proceedings/index.
[25] J. Beringer *et al.*, Phys. Rev. D **86**, 010001 (2012).